Orbital-selective nature of the 3d electronic structure of the ThFeAsN superconductor

L. Craco[1,2] and S. Leoni[3]

[1]*Institute of Physics, Federal University of Mato Grosso, Cuiabá, 78060-900 Mato Grosso, Brazil*
[2]*Leibniz Institute for Solid State and Materials Research Dresden, D-01069 Dresden, Germany*
[3]*School of Chemistry, Cardiff University, Cardiff CF10 3AT, United Kingdom*

Based on local-density approximation plus dynamical mean-field theory (LDA + DMFT) calculations, we perform a comprehensive analysis of electronic structure reconstruction of the ThFeAsN superconductor, showing how the normal and *s* wave superconducting spectra are reshaped by many-particle electron-electron interactions. Here, the ThFeAsN parent compound is described as an orbital-selective marginal Fermi liquid metal, with coexisting Fermi liquid quasiparticles and pseudogapped electronic states. Upon electron doping, an additional Kondo insulating state is predicted to exist in this system. Furthermore, we show how dynamical correlations strongly renormalize the bare Bogoliubov quasiparticles in the *s* wave superconducting state into totally correlated lineshapes. These findings contribute to the microscopic understanding of the role played by dynamical multiorbital electronic correlations in the low energy spectrum relevant to unconventional Fe-based superconductors.

I. INTRODUCTION

The emergence of unconventional superconductivity in layered Fe materials [1–4] has been at the forefront of condensed matter and materials science for more than a decade now. Much has been learned about the origin and intertwined roles of different phases in this class of correlated electron systems, in addition to the role played by intrinsic orbital selectivity, magnetism, nematicity, and pairing superconducting symmetry. In particular, the outstanding and vigorous debates concerning the nature of the normal state giving way to unconventional superconductivity have also influenced the discussion about the normal state electronic structure and the mechanism(s) of structural and magnetic phase instabilities. One of the central questions has been understanding whether superconductivity results as a pairing instability of a Fermi liquid metal, or as one of a marginal Fermi liquid [5] near an orbital-selective Mott metal-insulator transition [6]. Clearly, one possible way to resolve this question is to systematically investigate as many members of the Fe-based family as possible. To date, both normal magnetically ordered and nematic phases have been studied in various members of the family [1,4]. This has eventually shown that, in their normal paramagnetic state, the Fe-based superconductors (both pnictides and chalcogenides) increasingly fall into the bad-metal category [7], where the electrical resistivity [$\rho(T)$] deviates considerably from the canonical Fermi liquid T^2 behavior as $T \rightarrow 0$. Usually, in strongly correlated electron systems, the generic picture is known to be one where $\rho(T)$ displays a T^n power-law behavior in the bad-metal state with $1 < n < 2$. This is due to the development of a severely renormalized lattice coherence scale, driven by the increasing relevance

of dynamical multiorbital (MO) electronic correlations as T reduces. Thus, starting from the early days of the iron age [8], it has now being recognized that in this anomalous class of superconducting materials the Fermi liquid behavior is not recovered, even when superconductivity is suppressed by appropriate perturbations. Moreover, optical and spectroscopic studies in most Fe-based superconductors show large-scale spectral weight transfer (SWT) as a function of electron/hole doping, pressure, and temperature across the magnetic and superconducting phase instabilities, which once more is a fingerprint of correlated electrons near Mott localization. $\rho(T) \approx T^n (1 < n < 2)$ and the absence of Drude peak above T_c are features shared, along with different quantum critical metals [2,9,10]. Thus, the marginal Fermi liquid metallic state [5] has pointed in the direction of a fundamental role played by the electronic structure reconstruction of quantum critical bad metals.

In this context, finding superconductivity [11] followed by $\rho(T) = T^{1.3}$ behavior from 150 K down to temperatures close to $T_c = 30$ K in ThFeAsN [12] is interesting, since it adds an additional member within the 1111 family of Fe-based superconductors, where superconductivity emerges in the parent compound at ambient pressure. Similar to the LiFeAs superconductor, ThFeAsN has no structural phase instability, in contrast to the structural transition from the high-T tetragonal to low-T orthorhombic phase found in most of Fe-based superconductors [1]. Although strong magnetic fluctuations above 35 K have been reported [13], ThFeAsN shows unconventional superconductivity without antiferromagnetism, even in the absence of chemical doping and other treatings [11,14]. We recall here that band structure calculation predicts that undoped ThFeAsN should show stripe antiferromagnetic

075110-1

order similar to 1111 Fe-pnictides [15,16]. Thus, the absence of this fundamentally important feature indicates a sizable low-energy electronic structure reconstruction in ThFeAsN. The simultaneous presence of spin fluctuations and lack of magnetic order places ThFeAsN in the same class with LiFeAS and FeSe superconductors [13], which also show sizable MO electron-electron correlation effects [17,18], albeit without magnetically ordered ground states. We notice, however, that LiFeAs is considered to be a weakly correlated Fermi liquid metal with an onsite Coulomb interaction U close to 2.5 eV [18]. On the other hand, FeSe is on the strongly correlated side of the U to bare bandwidth (W) phase diagram [19], showing a pseudogapped normal electronic state at low T [17]. As shown below, ThFeAsN is slightly more correlated compared to LiFeAs, thus helping to refine the fundamental debate [20] on the relationship between the degree of electronic correlations and the proximity to orbital-selective Mott localization in Fe-based superconductors in general.

It is worth mentioning here that the consequences of orbital selectivity in ThFeAsN has not received the attention it deserves. Motivated by this, in this work we analyze the electronic structure reconstruction induced by dynamical MO electronic correlations in the Fe-3d shell of ThFeAsN. As shown below, all five 3d bands must be considered in order to satisfactorily resolve the bad-metallic electronic state obtained in pure and electron-doped regimes. In bad metals close to selective Mott localization, sizable electronic correlations drives interesting physical effects upon changes of bare bandwidth, many-particle interactions, and doping. These tunable degrees of freedom can induce an exotic regime, where the chemical potential lies in an energy region of almost vanishing density-of-states (DOS), naturally yielding coexistent metallic, insulating, and pseudogapped electronic states. In this work, we use the local-density approximation plus dynamical mean-field theory (LDA + DMFT) [21] to study these issues in the normal and s-wave superconducting state [13] of ThFeAsN. We also discuss the influence of orbital selectivity on the issues mentioned above, and follow this up with specific predictions which can be tested in future experiments.

II. RESULTS AND DISCUSSION

MO physics is inherently complex due to lattice, charge, and spin degrees of freedom [19]. These coupled correlations have hampered fully realistic theoretical studies so far. Density functional plus dynamical mean-field theory (DFT + DMFT) [21] allows for a systematic approach to the treatment of MO electronic correlations. Here, LDA calculations for the tetragonal crystal structure (see Fig. 1) of ThFeAsN (space group symmetry $P4/nmm$) were performed using the linear muffin-tin orbitals (LMTO) [22] scheme in the atomic sphere approximation. Experimental lattice parameters $a = 4.0367(1)$ Å and $c = 8.5263(2)$ Å were used as inputs to our first principles DFT calculations [11]. The two free crystal coordinates z_{As} and z_{Th} were 0.6388 and 0.1382, respectively. The total density was converged on a grid of 315 irreducible k points, and the radii of the atomic spheres were chosen as $r = 2.617$ (Fe), $r = 3.245$ (Th), $r = 2.122$ (N), and $r = 2.756$ (As) a.u. in order to minimize their overlap. As a result, the corresponding or-
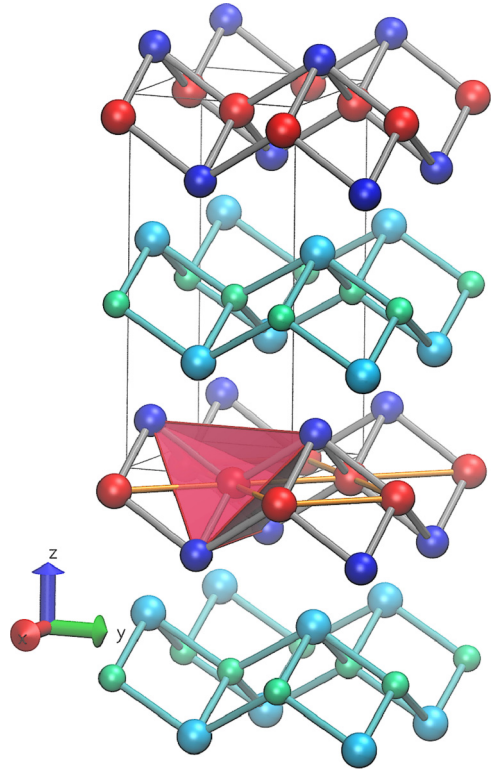
FIG. 1. Crystal structure of tetragonal ThFeAsN superconductor (Fe red, As blue, Th light-blue, N green). The tetragonal coordination of Fe by As is represented as a red tetrahedron. Within a single layer, the square planar arrangement of Fe atoms is shown (orange connections). The tetragonal unit cell is drawn in gray.

bital resolved LDA DOS is displayed in Fig. 2, showing good agreement with extant calculations [23]. Consistent with earlier band structure calculations for tetragonal Fe superconductors, the lineshape of the bare DOS is strongly orbital dependent, showing semiconducting ($3z^2 - r^2$), semimetallic (xy), and metallic electronic states with $xz, yz, x^2 - y^2$ orbital character near the Fermi level, $E_F = \omega = 0.0$.

The one-electron part of the Fe-3d model Hamiltonian relevant to ThFeAsN superconductor is $H_0 = \sum_{\mathbf{k},a,\sigma} \epsilon_a(\mathbf{k}) c^{\dagger}_{\mathbf{k},a,\sigma} c_{\mathbf{k},a,\sigma}$, where $a = x^2 - y^2, 3z^2 - r^2, xz, yz, xy$ denotes its 3d orbitals and $\epsilon_a(\mathbf{k})$ is the corresponding band dispersion, which encodes details of the one-electron (DFT) band structure. These five Fe-3d bands are the relevant one-particle inputs for MO-DMFT, which generates a strongly renormalized electronic state as shown below. Similar to earlier studies [8,17,18], the correlated many-body Hamiltonian relevant to ThFeAsN reads $H_{int} = U \sum_{i,a} n_{i,a,\uparrow} n_{i,a,\downarrow} + U' \sum_{i,a \neq b} n_{i,a} n_{i,b} - J_H \sum_{i,a \neq b} \mathbf{S}_{i,a} \cdot \mathbf{S}_{i,b}$. Here, U is the onsite Coulomb interaction, $U' = U - 2J_H$ is the interorbital Coulomb interaction term, and J_H is the Hund's coupling. Given the complexity of the MO problem, with diagonal and off-diagonal lattice Green's functions and self-energies [24], here we work in the basis which diagonalizes the one-particle density matrix. In this basis interorbital one-electron overlap is zero, and so in the paramagnetic phase we have $G_{a,b,\sigma}(\omega) = \delta_{a,b} G_{a,\sigma}(\omega)$ [25].
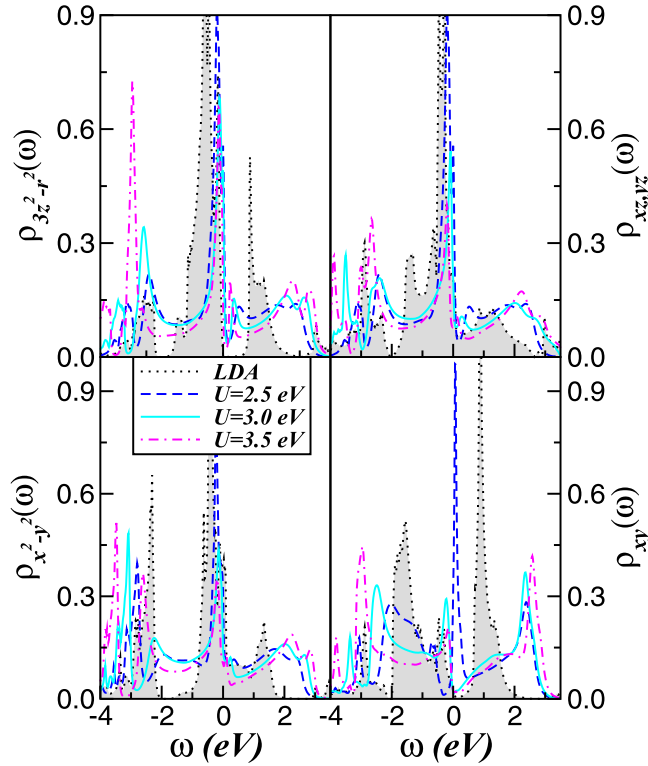
FIG. 2. LDA and LDA + DMFT orbital resolved density-of-states (DOS) of a tetragonal ThFeAsN superconductor, showing spectral weight redistribution over large energy scales with increasing onsite Coulomb interaction U. While all orbitals are metallic at $U = 2.5$ eV, orbital-selective localization within the xy orbital sets in for $U = 3.0$ eV. Particular interesting features to be seen are the peak-dip-hump within the $3z^2 - r^2$, xy, yz, $x^2 - y^2$ orbitals and the local moment (lower Hubbard band) formation in the $3z^2 - r^2$ orbital at $U = 3.5$ eV.

In this regime electrons among different orbitals interact only via interorbital Coulomb correlation and Hund's coupling effects [26]. We evaluate the retarded Green's functions $[G_a(\mathbf{k}, \omega) = \frac{1}{\omega - \Sigma_a(\omega) - \epsilon_a(\mathbf{k})}$, with $\Sigma_a(\omega)$ being the Fe-3d self energy of orbital a] of the hidden many-particle problem of ThFeAsN using the multiorbital iterated perturbation theory (MO-IPT) as an impurity solver to single-site DMFT. The full set of equations for the MO case can be found, for example in Ref. [26], therefore we do not repeat the equations here. This real frequency perturbative ansatz has a proven record of good semiquantitative agreement with experiments for a range of correlated materials, and it gives results in qualitatively accord with numerical exact continuos-time quantum Monte Carlo (CT-QMC) calculations [27].

Since the effect of electronic correlations in the excitation spectrum of ThFeAsN is not fully understood yet, in Fig. 2 we compare the LDA and the reconstructed orbital-resolved spectral functions that emerge from dynamical MO correlations in the bulk. Here we use values between 2.5 to 3.5 eV for the Fe-3d shell, recently considered for the parent LiFeAs and FeSe superconductors [18,27], to explore the electronic structure evolution with increasing the onsite Coulomb interaction U and fixed $J_H = 0.7$ eV. Upon consideration of MO

dynamical correlations, the sharp and well defined features of the bare electronic structure [23] are smeared within the energy window of ± 3 eV, clearly visible in Fig. 2. Many-particle MO self-energy corrections, induced using an onsite Coulomb interaction ($U = 2.5$ eV) similar to that considered for LiFeAs [18], lead to the emergence of lower (LHB) and upper (UHB) bands in the valence, and conduction bands at energies above ± 2.0 eV on all orbitals for the d^6 (Fe^{2+}) electronic configuration of undoped ThFeAsN. While some sharp features remain visible at high binding energies, the overall spectra is considerably broad as compared to the bare spectral functions. Interestingly, at $U = 2.5$ eV all orbitals reveal narrow Fermi liquid quasiparticles [28] at low energies. However, at $U = 3.0$ eV orbital-selective incoherence emerges in tetragonal ThFeAsN, which is characterized by a pseudogapped electronic state within the xy orbital at low energies. While the less correlated orbitals show peak-dip-hump [29] structures near E_F, the xy orbital is found to be very close to orbital-selective Mott localization for $U = 3.5$ eV, with most of its spectral weight being transferred to the Hubbard bands at high energies. Also interesting, in Fig. 2 is the strongly localized moment (LHB) which emerges in the $3z^2 - r^2$ orbital at $U = 3.5$ eV, suggesting that an antiferromagnetically ordered state could be seen in strained ThFeAsN crystals due to enhanced U/W ratio via strain-induced one-particle band narrowing. Taken together, our results at U close to 3.0 eV in Fig. 2 reveal the coexistence of narrow Kondo quasiparticles and strongly incoherent electronic states with xy orbital character in ThFeAsN. Future polarized x-ray emission and absorption spectroscopy studies are called for to confirm our prediction for the renormalized normal electronic spectrum of the undoped ThFeAsN superconductor.

To further characterize the correlated nature of the paramagnetic normal state, in Fig. 3 we show the U dependence of the self-energy imaginary (main panels) and real (insets) parts associated with the active Fe 3d-orbitals of ThFeAsN. Comparing our results to that of tetragonal FeSe superconductor [27], we notice similar features despite different orbital character in both systems, i.e., a clearly visible particle-hole asymmetry in $\Sigma_a(\omega)$, which is intensified with increasing U. This particle-hole asymmetry is also manifested in the self-energy real parts. Interesting as well is the appearance of a peak close to E_F in $Re\Sigma_{xy}(\omega)$, which is strongly enhanced with increasing U. Such frequency dependence suggests that the selective Mott localization of ThFeAsN is governed by the strong frequency dependence of the self-energy real and imaginary parts. In the orbital-selective bad-metal regime a remarkable aspect stands out: $Im\Sigma_{xy}(\omega)$ nearly vanishes at low energies instead of having a pole, as would occur in a conventional Mott insulator. As pointed out in our earlier study [30], this aspect is somehow reminiscent of marginal Fermi liquids, where below the orbital-selective Mott localized phase only the degenerated xz, yz of orbitals of the FeS superconductor show characteristic Fermi liquid-like features, while the more correlated orbitals display deviations from the $-\omega^2$ Fermi liquid form at small ω, being consistent instead with (sub-) linear ω dependence of marginal Fermi liquids [5]. Similar to the self-energy behavior in Fig. 3, sublinear energy dependence was also found in tetragonal and pseudo-hexagonal FeSe [27] as well as in electron doped FeTe [31],
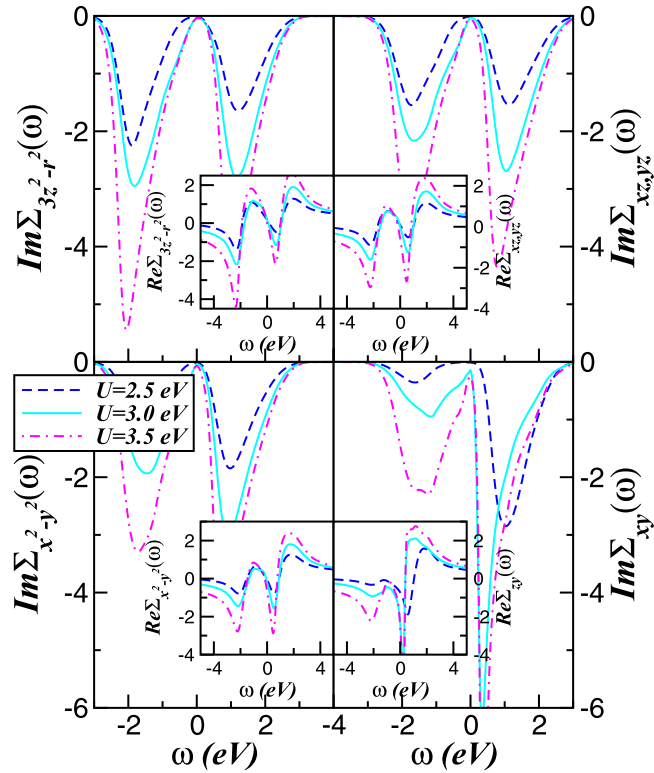
FIG. 3. Orbital-resolved self-energies imaginary (main panels) and real (insets) parts of ThFeAsN parent compound, showing their evolution with increasing U for fixed $J_H = 0.7$ eV. Particular features seen are the particle-hole asymmetry and the almost perfect Fermi liquid (ω^2) behavior of $Im\Sigma_a(\omega)$ ($a = 3z^2 - r^2, xz, yzx^2 - y^2$), suggesting the coexistence of itinerant electrons and nearly Mott localized electronic states with xy orbital character in the unconventional electronic fluid of ThFeAsN. Also interesting is the frequency dependence of the self-energy real parts, showing orbital dependent electron correlation effects.

FIG. 4. Low energy view of orbital resolved spectral functions of pure and electron-doped ThFeAsN. Notice the robustness of the xy pseudogapped electronic state and the emergence of a Kondo insulating state with $3z^2 - r^2$ orbital character upon increasing the total electron band filling of the Fe-3d shell.

suggesting a common scenario of orbital-selective marginal Fermi liquidness in stoichiometric Fe-based superconductors. Finally, since in DMFT the self energy is momentum independent, the quasiparticle residue Z_a of an orbital a, which defines the renormalized Fermi energy, directly yields the effective electron mass enhancement: $\frac{m_a^\star}{m_e} = \frac{1}{Z_a} = (1 - \frac{\partial Re\Sigma_a(\omega)}{\partial \omega})_{\omega=0}$, where m_e is the free electron mass. Thus, from the slope of the self-energy real part we obtain for $U = 3.0$ eV and $n = 6.4$ (see our discussion below), $(\frac{m_{3z^2-r^2}^\star}{m_e}, \frac{m_{xz,yz}^\star}{m_e}, \frac{m_{x^2-y^2}^\star}{m_e}, \frac{m_{xy}^\star}{m_e}) = (2.6, 3.0, 3.6, 10.9)$, the former being in good accord with carrier's effective mass $m^* = 2.48m_e$ estimated from muon-spin rotation (μSR) measurements [32], attesting to the role played by electron correlation effects in the normal, paragmanetic state of ThFeAsN superconductor.

In order to get more insights into the normal state electronic structure reconstruction of ThFeAsN, in Fig. 4 we show the effect of electron-doping the parent compound. This is motivated by the fact that Hall data and crystal structure analyses suggest that the superconducting material behaves as an optimally electron-doped 1111 pnictide superconductor, due to extra electrons from nitrogen deficiency or oxygen occupancy at the nitrogen site [12]. Thus, what happens upon electron

doping the parent compound? Even though no spectroscopy data exist, the generic appearance of novel states and the instabilities of such states to unconventional order, and in particular to high temperature superconductivity, in a wide variety of other correlated electron systems makes this an important question to inquire about. Our aim here is to build upon the strengths of correlated electronic structure modeling to analyze the effect of electron doping in ThFeAsN. In particular, based on explicit calculations, we will present a set of predictions which could be tested in future experimental works in the normal as well as in the single gap s-wave superconducting state [13].

In Fig. 4 we show the changes in the correlated electronic structure upon electron doping ($n = 6 + \delta$, with $\delta > 0$) ThFeAsN parent compound. An intriguing observation is that the pseudogap localization-delocalization transition does not occur at small doping within the xy orbital, showing the robustness of the pseudogapped regime to electron doping. However, as δ increases, a selective-Kondo insulating state develops in the $3z^2 - r^2$ spectral function, showing a crossover from a metal to a Kondo insulator with almost vanishing DOS at E_F for $n = 6.4$. While the $xz, yz, x^2 - y^2$ orbitals display metallic behavior, this is a clear demonstration of orbital-selective electronic reconstruction in electron doped ThFeAsN. What is the origin of these features? In a MO system like ThFeAsN, scattering between different carriers in orbital states lineshape leads to two main effects: orbital-dependent shifts of the 3d-bands relative to each other via static-Hartree contributions (from the static part of the orbital-dependent self-energies), and strong dynamical correlations due to sizable U, U', and J_H which cause appreciable SWT over large energy scales (not shown in Fig. 4) upon carrier doping. This second feature leads to an orbital-selective modification of the spectral functions at low energies, as shown in Fig. 4. Thus, for electron-doped ThFeAsN, coexisting pseudogapped and Kondo components should be visible at low

energies, in spite of large scale dynamical SWT. These are stringent tests for our proposal, and experimental verification should place it on solid ground.

It should be noted that Kondo insulators are correlated systems [33] whose excitations and normal state properties are adiabatically connected to noninteracting semiconductors [34]. Hence, they can be seen as an analytically continued version of conventional band insulators, where sizable correlations do exist above the one-particle gap scale. In Kondo insulators when the band filling is slightly different from its commensurate value, a coherent electronic cloud is created close to (E_F), and the resulting metallic state (in absence of disorder or proximity to quantum criticality) is Fermi liquid. On the other hand, in effectively Mott-localized systems the insulating state arises because electron hopping from one site to another is inhibited by strong Coulomb repulsions [35]. In Mott systems, electron hopping is drastically reduced or blocked altogether, and the resulting metallic state upon doping can vary from a Fermi liquid to an orbital-selective non-Fermi liquid metal depending on the band structural details, strength of onsite electron-electron interactions, doping, and temperature [36].

Incoherent bad metallicity with clear deviation from the Fermi liquid T dependence of the resistivity, $\rho(T) = T^n$ with $n = 1.3$ [12], as shown below, may provide additional support to our orbital-selective electronic structure of ThFeAsN superconductor. Specifically, we study the T dependence of the dc resistivity and correlate it with the orbital-reconstruction scenario derived above. Given the correlated spectral functions $A_a(\mathbf{k}, \omega) = -\frac{1}{\pi} Im G_a(\mathbf{k}, \omega)$, the (static) dc conductivity [$\sigma_{dc}(T)$], computed within the DMFT formalism, [37] can be expressed as $\sigma_{dc}(T) = \frac{\pi}{T} \sum_a \int d\epsilon \rho_a^{(0)}(\epsilon) \int d\omega A_a^2(\epsilon, \omega) f(\omega)[1 - f(\omega)]$. In this expression, $\rho_a^{(0)}(\epsilon)$ is the LDA DOS of the a bands (Fig. 2) and $f(\omega)$ is the Fermi function.

In Fig. 5 we display the T dependence of electrical resistivity [$\rho_{dc}(T) \equiv 1/\sigma_{dc}(T)$], computed using the LDA + DMFT orbital resolved spectral functions for in $\sigma_{dc}(T)$. For further consistency with experiments, we display in the main panel of Fig. 5 the effect of electron-doping on the dc resistivity of ThFeAsN parent compound, showing appreciable doping dependence below 100 K. As seen, for $n = 6.0$ the resistivity has nearly linear T dependence down to low temperatures. With increasing n, we observe a slight upturn below about 11 K for $n = 6.2$, followed by a S-like shape at $n = 6.4$, which is characteristic of pseudogapped metals [17]. Interestingly, with increasing the band filling $\rho(T)$ becomes more insulating-like, smoothly approaching the incipient saturating-like behavior above 300 K. Moreover, as seen in the inset of Fig. 5, LDA + DMFT (MO-IPT) provides a compelling description of observed experimental data above T_c [11,12], supporting the role of sizable electronic correlations in Fe-based superconductors in general. In an earlier study [17], the origin of the S-like form found in ThFeAsN for $n = 6.4$ has been clarified microscopically. Therein, it was shown that orbital-selective incoherence characterizes the paramagnetic phase in a layered FeSe superconductor. According to our LDA + DMFT results, the emergence of a S-like form below 50 K should be considered as a manifestation of slightly increasing the band filling (via intrinsic
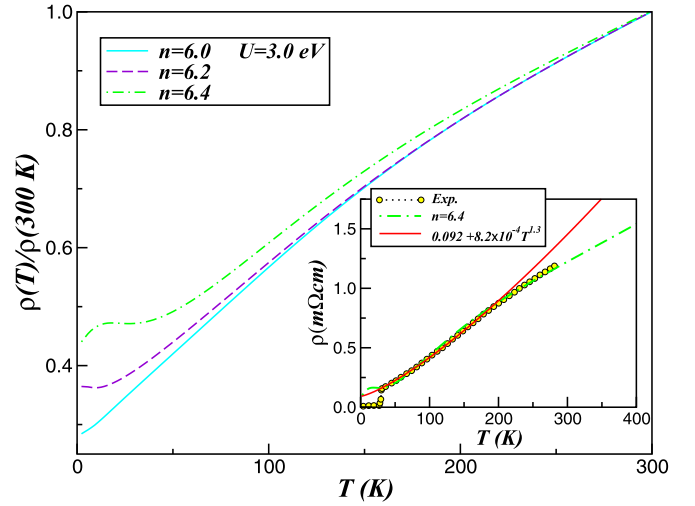
FIG. 5. T dependence of electrical resistivity (normalized at 300 K) for pure and electron-doped ThFeAsN, showing visible doping dependence below 100 K. Inset: theory-experiment comparison of resistivity versus temperature normalized to the experimental value at $T_c = 30\,\mathrm{K}$ [11,12]. Notice the good agreement between theory, experiment, and the fitting curve from 215 K down to T_c.

self-doping [38], or, as in the case of ThFeAsN, via nitrogen deficiency or oxygen occupancy at the nitrogen site) [12], an orbital-selective metal close to orbital-selective electronic localization. The fact that $\rho(T)$ substantially increases between $n = 6.2$ and 6.4 implies that an emergent Kondo insulating state with $3z^2 - r^2$ orbital character is promoted on increasing the carrier concentration of the Fe 3d-shell, as shown in Fig. 4.

In order to shine light onto the changes in the excitation spectrum of bulk ThFeAsN across the superconducting phase transition, we have extended our normal state electronic structure calculation to analyze the role played by the single s-wave gap [13] within LDA + DMFT formalism for the superconducting state. Given the complexity of the problem [32], here we assume that pair formation primarily involves the active xz, yz orbitals due to their intrinsic orbital degeneracy, favoring particle-hole (nematic or antiferromagnetic order) and particle-particle (MO superconductivity) instabilities [39]. Using this assumption and the s-wave superconducting pair-field Δ, the LDA + DMFT equations for the xz, yz orbitals are readily extendable to the superconducting regime. In the superconducting phase, the one-particle Green's function have normal and anomalous components, yielding renormalized $G_{a,\sigma}$ propagators which are solved by extending the normal state LDA + DMFT solution to include an explicit pair potential term [40]. Including the s-wave pair-field Δ, the LDA + DMFT propagators for the $a = xz, yz$ orbitals are written as [41]

$$G_{a,\sigma}(\omega, \mathbf{k}) = \frac{1}{\omega - \Sigma_{a,\sigma}(\omega) - \varepsilon_a(\mathbf{k}) - \frac{\Delta^2}{\omega + \Sigma_{a,\bar{\sigma}}^*(\omega) + \varepsilon_a(\mathbf{k})}},$$

where the $*$ denotes complex conjugation. Within our assumption, ThFeAsN can be thought of as two 3d electronic fluids, one which participates in the superconducting state and another one which does not. As such, our two-fluid scenario should be applicable to superconductors with orbital
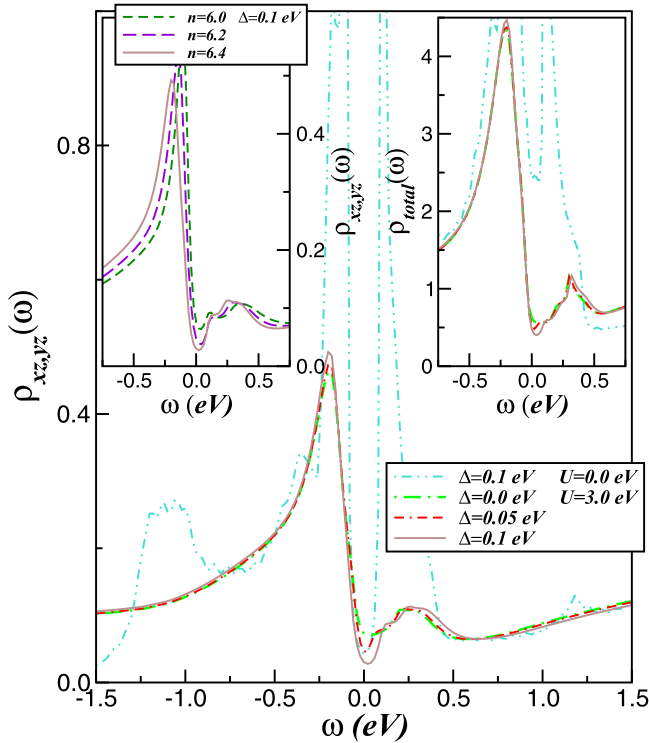
FIG. 6. xz, yz and total spectral functions in the single gap s-wave superconducting state [13] of a bulk ThFeAsN crystal, showing their evolution with changing the pair-field Δ and fixed $n = 6.4$ (main and right inset panels), and by enhancing the electron band filling with fixed $\Delta = 0.1$ eV (left inset panel). Notice the particle-hole asymmetry and the nearly similar correlated spectral functions at low energies. Also noteworthy are the Bogoliubov quasiparticles obtained in the $U = 0.0$ eV limit, which are strongly reshaped due to dynamical spectral weight transfer induced by multiorbital electron interactions at energies above the s-wave superconducting gap.

degeneracy, where a portion of the normal spectral weight participates in the superconducting condensate below T_c. In this perspective, our findings below open up interesting avenues for future studies on two-fluid theories of superconductivity [42].

We now describe our results within the single s-wave gap superconducting state [13] of bulk ThFeAsN. Using the $U = 0.0$ eV solution for $\Delta = 0.1$ eV and $n = 6.4$ we show the emergent low energy electronic lineshape induced by superconductivity in the active xz, yz spectral functions in the main panel of Fig. 6. Clear appearance of a superconducting gap and sharp singularities at low energies are induced by the superconducting instability in the $3d_{xz,yz}$ orbital sector. The emergence of sharp singularities at low energies as in Fig. 6, the so-called Bogoliubov quasiparticles, is the fingerprint of conventional s-wave superconductivity [43]. Remarkable,

however, are our finite U results, showing substantial renormalization of the asymmetric Bogoliubov quasiparticles. As seen, apart from the s-wave gap structure, the reconstructed electronic state above the superconducting gap is very similar to that found in the normal state. This is strictly tied to the fact that in ThFeAsN the excitation spectrum of the xz, yz orbitals is already strongly renormalized by $U = 3.0$ eV for $n = 6.4$, as shown in Fig. 4. Additionally, in the left inset of Fig. 6 we show the effect of electron doping in the s-wave superconducting state. As seen, appreciable SWT from low to high energies occurs, which in turn enhances the superconducting gap upon increasing the total band filling of the Fe-$3d$ shell. Finally in the right inset of Fig. 6 we display the computed total spectral functions of superconducting ThFeAsN for $n = 6.4$, showing similar SWT to that found for total spectral function of an F-doped LaFeAsO superconductor [40], implying that MO electronic correlations intrinsically govern the nature of the electronic spectra of unconventional (s-wave or not) superconductors. Future tunneling and spectroscopy measurements are called for to corroborate our two-fluid superconducting scenario and the changes in the total one-particle spectral function across the single gap [13] s-wave superconducting transition in ThFeAsN.

III. CONCLUSION

In conclusion, we have studied the instability of the orbital-selective normal state of ThFeAsN to a single gap [13] s-wave superconducting instability. Extending earlier LDA + DMFT calculations for the orbital-selective bad metal, we find good qualitative power-low T-dependence agreement for electron-doped ThFeAsN with extant electrical transport data [12]. At low energies absence of sharp Bogoliubov quasiparticles in the valence and conduction band spectrum for the s-wave phase, as well as weak spectral weight transfer across the superconducting transition, is obtained. Further, possible proximity effects with competing states exhibiting sizable spin fluctuations [13], not included in our theory, might offer additional low energy features to be seen in future spectroscopy and tunneling studies.

[1] D. C. Johnston, Adv. Phys. **59**, 803 (2010); G. R. Stewart, Rev. Mod. Phys. **83**, 1589 (2011); E. Dagotto, *ibid.* **85**, 849 (2013).

[2] Q. Si, R. Yu, and E. Abrahams, Nat. Rev. Mat. **1**, 16017 (2016).

[3] M. Yi, Y. Zhang, Z.-X. Shen, and D. Lu, npj Quantum Mater. **2**, 57 (2017).

[4] A. Kreisel, P. J. Hirschfeld, and B. M. Andersen, Symmetry **12**, 1402 (2020).

[5] C. M. Varma, P. B. Littlewood, S. Schmitt-Rink, E. Abrahams, and A. E. Ruckenstein, Phys. Rev. Lett. **63**, 1996 (1989); G. R. Stewart, Rev. Mod. Phys. **73**, 797 (2001)

[6] L. de'Medici, G. Giovannetti, and M. Capone, Phys. Rev. Lett. **112**, 177001 (2014).

[7] X. Deng, J. Mravlje, R. Žitko, M. Ferrero, G. Kotliar, and A. Georges, Phys. Rev. Lett. **110**, 086401 (2013).

[8] L. Craco, M. S. Laad, S. Leoni, and H. Rosner, Phys. Rev. B **78**, 134511 (2008).

[9] E. Abrahams and Q. Si, J. Phys.: Condens. Matter **23**, 223201 (2011); J. A. N. Bruin, H. Sakai, R. S. Perry, and A. P. Mackenzie, Science **339**, 804 (2013); J. Vučičević, D. Tanasković, M. J. Rozenberg, and V. Dobrosavljević, Phys. Rev. Lett. **114**, 246402 (2015); S. Licciardello, J. Buhot, J. Lu, J. Ayres, S. Kasahara, Y. Matsuda, T. Shibauchi, and N. E. Hussey, Nature **567**, 213 (2019).

[10] N. Maksimovic, I. M. Hayes, V. Nagarajan, A. E. Koshelev, J. Singleton, Y. Lee, T. Schenkel, and J. G. Analytis, Phys. Rev. X **10**, 041062 (2020).

[11] C. Wang, Z.-C. Wang, Y.-X. Mei, Y.-K. Li, L. Li, Z.-T. Tang, Y. Liu, P. Zhang, H.-F. Zhai, Z.-A. Xu, and G.-H. Cao, J. Am. Chem. Soc. **138**, 2170 (2016).

[12] H. Mao, C. Wang, H. E. Maynard-Casely, Q. Huang, Z. Wang, G. Cao, S. Li, and H. Luo, Europhys. Lett. **117**, 57005 (2017).

[13] T. Shiroka, T. Shang, C. Wang, G.-H. Cao, I. Eremin, H.-R. Ott, and J. Mesot, Nat. Commun. **8**, 156 (2017).

[14] J. Wang, F. Jiao, X. Wang, S. Zhu, L. Cai, C. Yang, P. Song, F. Zhang, B. Li, Y. Li, J. Hu, S. Li, Y. Li, S. Tan, Y. Mei, Q. Jing, C. Wang, B. Liu, and D. Qian, Europhys. Lett. **130**, 67003 (2020).

[15] D. J. Singh, J. Alloys Compd. **687**, 786 (2016).

[16] G. Wang and X. Shi, Europhys. Lett. **113**, 67006 (2016).

[17] L. Craco and M. S. Laad, Eur. Phys. J. B **89**, 119 (2016).

[18] J. Fink, J. Nayak, E. D. L. Rienks, J. Bannies, S. Wurmehl, S. Aswartham, I. Morozov, R. Kappenberger, M. A. ElGhazali, L. Craco, H. Rosner, C. Felser, and B. Büchner, Phys. Rev. B **99**, 245156 (2019).

[19] M. Imada, A. Fujimori, and Y. Tokura, Rev. Mod. Phys. **70**, 1039 (1998).

[20] Q. Si, Nat. Phys. **5**, 629 (2009); M. M. Qazilbash, J. J. Hamlin, R. E. Baumbach, L. Zhang, D. J. Singh, M. B. Maple, and D. N. Basov, *ibid.* **5**, 647 (2009).

[21] G. Kotliar, S. Y. Savrasov, K. Haule, V. S. Oudovenko, O. Parcollet, and C. A. Marianetti, Rev. Mod. Phys. **78**, 865 (2006).

[22] O. K. Andersen, Phys. Rev. B **12**, 3060 (1975); V. Antonov, B. Harmon, and A. Yaresko, *Electronic Structure and Magneto-Optical Properties of Solids* (Kluwer Academic Publishers Dordrecht, Boston, London, 2004).

[23] S. Sen and G.-Y. Guo, Phys. Rev. Mater. **4**, 104802 (2020); Phys. Rev. B **102**, 224505 (2020).

[24] See, for example, A. Koga, N. Kawakami, T. M. Rice, and M. Sigrist, Phys. Rev. B **72**, 045128 (2005).

[25] L. Craco, M. S. Laad, S. Leoni, and E. Müller-Hartmann, Phys. Rev. B **70**, 195116 (2004).

[26] L. Craco, Phys. Rev. B **77**, 125122 (2008).

[27] L. Craco and S. Leoni, Phys. Rev. B **100**, 121101(R) (2019).

[28] A. Georges, G. Kotliar, W. Krauth, and M. J. Rozenberg, Rev. Mod. Phys. **68**, 13 (1996).

[29] P. K. Nag, R. Schlegel, D. Baumann, H.-J. Grafe, R. Beck, S. Wurmeh, B. Büchner, and C. Hess, Sci. Rep. **6**, 27926 (2016).

[30] L. Craco and S. Leoni, Sci. Rep. **7**, 46439 (2017).

[31] L. Craco, B. Xu, M. Fang, and B. Freelon, Phys. Rev. B **101**, 165107 (2020).

[32] D. Adroja, A. Bhattacharyya, P. K. Biswas, M. Smidman, A. D. Hillier, H. Mao, H. Luo, G.-H. Cao, Z. Wang, and C. Wang, Phys. Rev. B **96**, 144502 (2017).

[33] R. M. Martin and J. W. Allen, J. Appl. Phys. **50**, 7561 (1979).

[34] M. Dzero, K. Sun, V. Galitski, and P. Coleman, Phys. Rev. Lett. **104**, 106408 (2010).

[35] R. G. Moore, J. Zhang, V. B. Nascimento, R. Jin, J. Guo, G. T. Wang, Z. Fang, D. Mandrus, and E. W. Plummer, Science **318**, 615 (2007).

[36] L. Craco and S. Leoni, Phys. Rev. B **85**, 195124 (2012).

[37] K. Haule and G. Kotliar, New. J. Phys. **11**, 025021 (2009).

[38] Z. P. Yin, K. Haule, and G. Kotliar, Nat. Mater. **10**, 932 (2011).

[39] M. S. Laad, B. Freelon, and L. Craco, arXiv:1805.09628.

[40] M. S. Laad and L. Craco, Phys. Rev. Lett. **103**, 017002 (2009).

[41] L. Craco, M. S. Laad, and S. Leoni, Sci. Rep. **7**, 2632 (2017).

[42] J. Bardeen, Phys. Rev. Lett. **1**, 399 (1958).

[43] N. F. Q. Yuan and L. Fu, Phys. Rev. B **97**, 115139 (2018).